

SEARCH FOR A DISTANCE-DEPENDENT BARYONIC TULLY-FISHER RELATION AT LOW REDSHIFTS

ADITI KRISHAK¹ AND SHANTANU DESAI²

¹ Department of Physics, IISER-Bhopal, Madhya Pradesh, 462066, India
² Department of Physics, IIT Hyderabad, Kandi Telangana-502284, India

Version June 15, 2022

ABSTRACT

A recent work (Alesta *et al.* 2021) has found a statistically significant transition in the Baryonic Tully-Fisher relation (BTFR) using low redshift data ($z < 0.1$), with the transitions occurring at about 9 and 17 Mpc. Motivated by this finding, we carry out a variant of this analysis by fitting the data to an augmented BTFR, where both the exponent as well as normalization constant vary as a function of distance. We find that both the exponent and normalization constant show only a marginal variation with distance, and are consistent with a constant value, to within 2σ . We also checked to see if there is a statistically significant difference between the BTFR results after bifurcating the dataset at distances of 9 and 17 Mpc. We find that almost all the sets of subsamples obey the BTFR with χ^2/dof close to 1 and the best-fit parameters consistent across the subsamples. Only the subsample with $D < 17$ Mpc shows a marginal discrepancy (at 1.75σ) with respect to the BTFR. Therefore, we do not find any evidence for statistically significant differences in the BTFR at distances of 9 and 17 Mpc.

1. INTRODUCTION

The Tully-Fisher relation is an empirical relation between the optical luminosity of spiral galaxies (L) and the asymptotic rotation velocity (v), originally obtained using HI line widths, given by $L \propto v^4$ (Tully and Fisher 1977). This relation has been superseded by a related relation known as Baryonic Tully-Fisher relation (BTFR), where the luminosity is replaced by the total baryonic mass (M_b) (McGaugh *et al.* 2000a)

$$M_B = Av^4 \quad (1)$$

where M_B is the sum of gas and star mass and A is the normalization constant equal to Ga_0 , where $a_0 \sim 10^{-10} m/s^2$. The BTFR has a much smaller scatter than the traditional Tully-Fisher relation (McGaugh *et al.* 2000b; Verheijen 2001a; Zaritsky *et al.* 2014), and most of its observed scatter can be attributed to observational uncertainties (Lelli *et al.* 2016). The BTFR is known to be valid for a whole slew of galaxies besides spirals, such as low surface brightness and gas rich spiral galaxies, and it also works in cases where the classic T-F relation fails (Famaey and McGaugh 2012; McGaugh *et al.* 2021). A heuristic way of understanding the BTFR is by positing that the surface density (M/R^2) is constant (Aaranson *et al.* 1979; Donato *et al.* 2009). This surface density is known to be constant for a wide class of systems (Freeman 1970; Donato *et al.* 2009; Salucci 2019), although there are exceptions in the form of galaxy clusters and groups (Gopika and Desai 2020, 2021). The BTFR cannot be trivially predicted by the current Λ CDM model (Mayer *et al.* 2022) (although see Paranjape and Sheth (2021); Kaplinghat and Turner (2002)), but naturally follows as a consequence of Modified Newtonian dynamics (Famaey and McGaugh 2012; McGaugh 2014, 2020). However, most relativistic theories of MOND have been ruled out after the simultaneous EM-GW observations from GW170817 (Boran *et al.* 2018).

Given the profound implications of the BTFR for new physics, there have been many theoretical (Bekenstein and Sagi 2008; Limbach *et al.* 2008; Portinari and Sommer-Larsen 2007) and observational (Übler *et al.* 2017; Glowacki *et al.* 2021; Alesta *et al.* 2021) (and references therein) efforts to search for its evolution as a function of redshift. These searches have often led to contradictory results. However, all these works only compared the high redshift samples with the low redshift ones. There was no study exclusively devoted to the low redshift end of the BTFR. Motivated by these considerations, Alesta *et al.* (2021) (A21, hereafter) analyzed the BTFR data at low redshifts ($z \lesssim 0.1$) corresponding to the distance range $\in [1, 130]$ Mpc to search for sharp discontinuities in the slope and intercept. This could in turn be used to constrain the effective Newton's constant (G_{eff}). A21 considered a sample of 118 data points in the distance range 2–60 Mpc, collated from multiple sources (Verheijen 2001b; Walter *et al.* 2008; Lelli *et al.* 2016). They analyzed the aforementioned data to look for a transition in the evolution of BTFR, thereby constraining a possible evolution of G_{eff} , and to check if any putative variations can ameliorate the Hubble tension conundrum (Verde *et al.* 2019; Di Valentino *et al.* 2021; Bethapudi and Desai 2017).

A21 bifurcated the sample into two subsets based on a critical distance D_c . The BTFR was fit separately for each of the two subsamples based on χ^2 minimization, which includes an intrinsic scatter of 7.7%. A21 found 3σ discrepancies between the subsamples after the splitting the dataset at $D_c=9$ Mpc and 17 Mpc. Such a transition could either be a systematic or a transition in the value of effective Newton's constant. If interpreted as a change in Newton's constant,

A21 obtained $\frac{\Delta G_{eff}}{G_{eff}} \sim -10\%$, where the minus sign corresponds to weaker gravity in the past. Such a magnitude of transition in G is in accord with the model in [Marra and Perivolaropoulos \(2021\)](#) designed to resolve the Hubble conundrum. However, the observed variation is at odds with the bounds on variation of G ([Zyla et al. 2020](#); [Bhagvati and Desai 2022](#)). Note however that the best-fit BTFR parameters are still consistent between the two subsamples (See Table 2 of A21). They have also not considered the difference in number of data points between the two subsamples.

Nevertheless, in order to independently investigate the intriguing result in A21, we try to reproduce their claims using two independent ways. We first carry out a variant of this procedure where we search for a distance-dependent smooth variation in the BTFR. We then try to characterize the differences in the subsamples after bifurcating the dataset at 9 and 17 Mpc.

This manuscript is organized as follows. We describe our analysis of the BTFR to search for distance-dependent variation in section 2. In section 3, we describe our analysis of the BTFR by splitting the dataset, with the intrinsic scatter as a free parameter as well as for a fixed value of the intrinsic scatter (section 3.1). Finally, in section 4, we summarize the results of our analyses and the conclusions that we draw from the results.

2. ANALYSIS OF DISTANCE-DEPENDENT BTFR

We start with the classical BTFR:

$$M_B = Av^s \quad (2)$$

This equation can be expressed in the logarithmic form as:

$$\ln M_B = s \ln v + \ln A \quad (3)$$

or, $y = sx + b$, where $y \equiv \ln M_B$ and $x \equiv \ln v$. s gives the slope and $b \equiv \ln A$ is the intercept of the logarithmic BTFR.

To search for distance-dependent transitions in the BTFR, we introduce a linear distance-dependence in the slope and intercept terms:

$$y = (sD + c)x + bD + e \quad (4)$$

Thus, s and b encode the distance-dependent slope and intercept, respectively, in our variant of this analysis. The log-likelihood for the above equation can be expressed as ([Gopika and Desai 2020](#); [Pradyumna et al. 2021](#))

$$-2 \ln \mathcal{L} = \sum_i \ln(2\pi\sigma_i^2) + \sum_i \frac{[y_i - ((sD_i + c)x_i + bD_i + e)]^2}{\sigma_i^2} \quad (5)$$

where the index i runs over all data points in consideration. σ_i^2 incorporates uncertainties in observation of x , y , and D along with the intrinsic scatter σ_s . Therefore,

$$\sigma_i^2 = \sigma_{y_i}^2 + (sD_i + c)^2 \sigma_{x_i}^2 + (sx_i + b)^2 \sigma_{D_i}^2 + \sigma_s^2 \quad (6)$$

Note that unlike A21, which fixed the scatter to a constant value of 7.7%, we kept the intrinsic scatter (σ_s) as a free parameter. With the data points provided in A21, we perform parameter optimization using MCMC, using the `emcee` sampler ([Foreman-Mackey et al. 2013](#)) for the model parameters s , c , b , and e . We used uniform priors across $[-100, 100]$ for s , c , b , and e . A log-uniform prior between 10^{-5} and 1 was used for σ_s . The marginalized 68% and 95% credible interval contours for each of the free parameters were obtained using the `getdist` ([Lewis 2019](#)) package.

The aforementioned marginalized credible intervals can be found in Fig. 1. We find that the best-fit values for s and b are given by $s = -0.0078 \pm 0.0054$ and $b = 0.02 \pm 0.012$. This shows that s and b are only marginally discrepant with respect to a constant value, at 1.4σ and 1.6σ , respectively. Therefore, prima-facie there is no evidence for a distance-dependent slope or normalization in the BTFR, when considering low-redshift data. We also find a strong degeneracy (anti-correlation) between b and s , as well as between e and c . The intrinsic scatter is given by $\ln \sigma = -1.54 \pm 0.2\%$, corresponding to about 20%. The best-fit values is shown on top of the data in Fig. 2.

3. ANALYSIS OF BTFR AFTER SPLITTING THE DATASET

One possible reason for the discrepancy with respect to A21 is that our previous analysis may not be sensitive to a step function in the values of BTFR parameters at fixed distances. Therefore, instead of looking for a smooth distance-dependent BTFR parameters, we divide the dataset into two distinct subsamples at distances of 9 Mpc and 17 Mpc, since A21 had found about 3.5σ difference between the BTFR parameters at these bifurcation points.

For each of these subsamples, we fit the classical BTFR (Eq. 3) using the same Gaussian likelihood as was used for our distance-dependent BTFR fits. Again, we keep the intrinsic scatter as a free parameter. Our results for the different datasets can be found in Table 1. We can see that the best-fit values for the slope and intercept, (which correspond to the normalization and exponent in the BTFR, respectively) are consistent between the two subsamples at 1σ . The intrinsic scatter is also consistent across the subsamples. Therefore, again we do not find any tension between the BTFR parameters after bifurcating the dataset based on distances corresponding to 9 and 17 Mpc. The last two columns in Table 1 show the best-fit χ^2 values and p -value, where χ^2 is calculated as follows:

$$\chi^2 = \sum_i \frac{[y_i - (sx_i + b)]^2}{\sigma_i^2}, \quad (7)$$

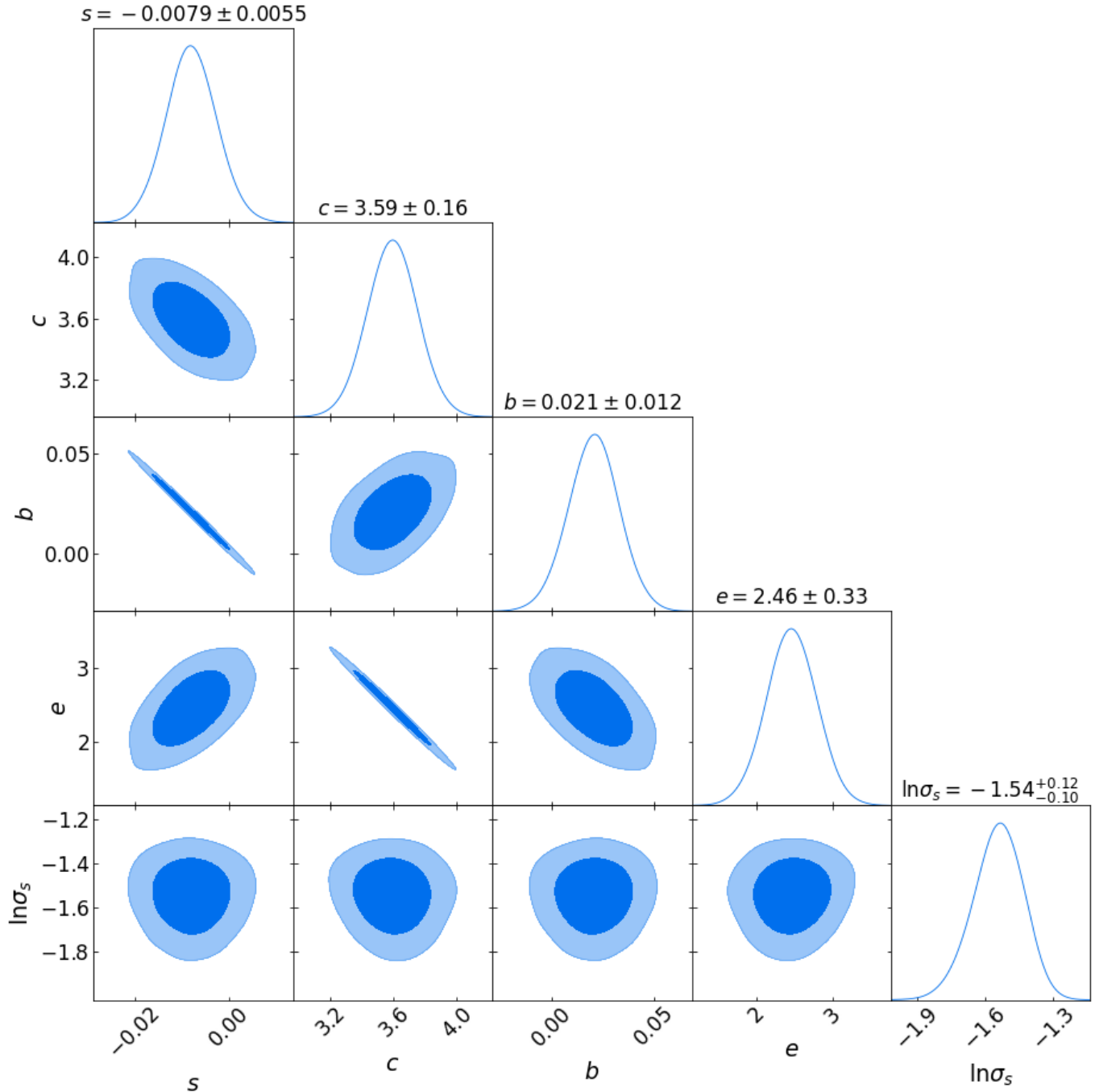


FIG. 1.— The marginalized 68% and 95% credible intervals for all the free parameters in Eq. 4. The contours have been produced using the `getdist` package in Python.

where s and b are the best-fit values for the slope and intercept ($b \equiv \ln A$), respectively. Although the χ^2 between the two subsamples differ, the dof (degrees of freedom) are different because of the difference in the number of data points. Therefore, instead of looking at difference in the χ^2 values between the subsamples as in A21, we consider the χ^2 p -value for each of the subsamples (Desai 2016). These p -values can be found in the last column of Table 1. All four subsamples have p -value close to 1. the χ^2/dof is also less than 1 for all subsamples. Therefore, there is no statistically significant differences between the subsamples.

3.1. Analysis using a fixed intrinsic scatter

Finally, we redo the analysis of BTFR (Eq. 3) using a fixed intrinsic scatter, instead of having it as a free parameter. We used the same value as A21 ($\sigma_s = 0.0077$), which was obtained by positing that χ^2/dof was equal to one. The results from this analysis can be found in Table 2. Once again, the best-fit parameters are consistent between the complementary subsamples within 1σ . If we compare the datasets obtained after splitting the samples at 9 Mpc, we

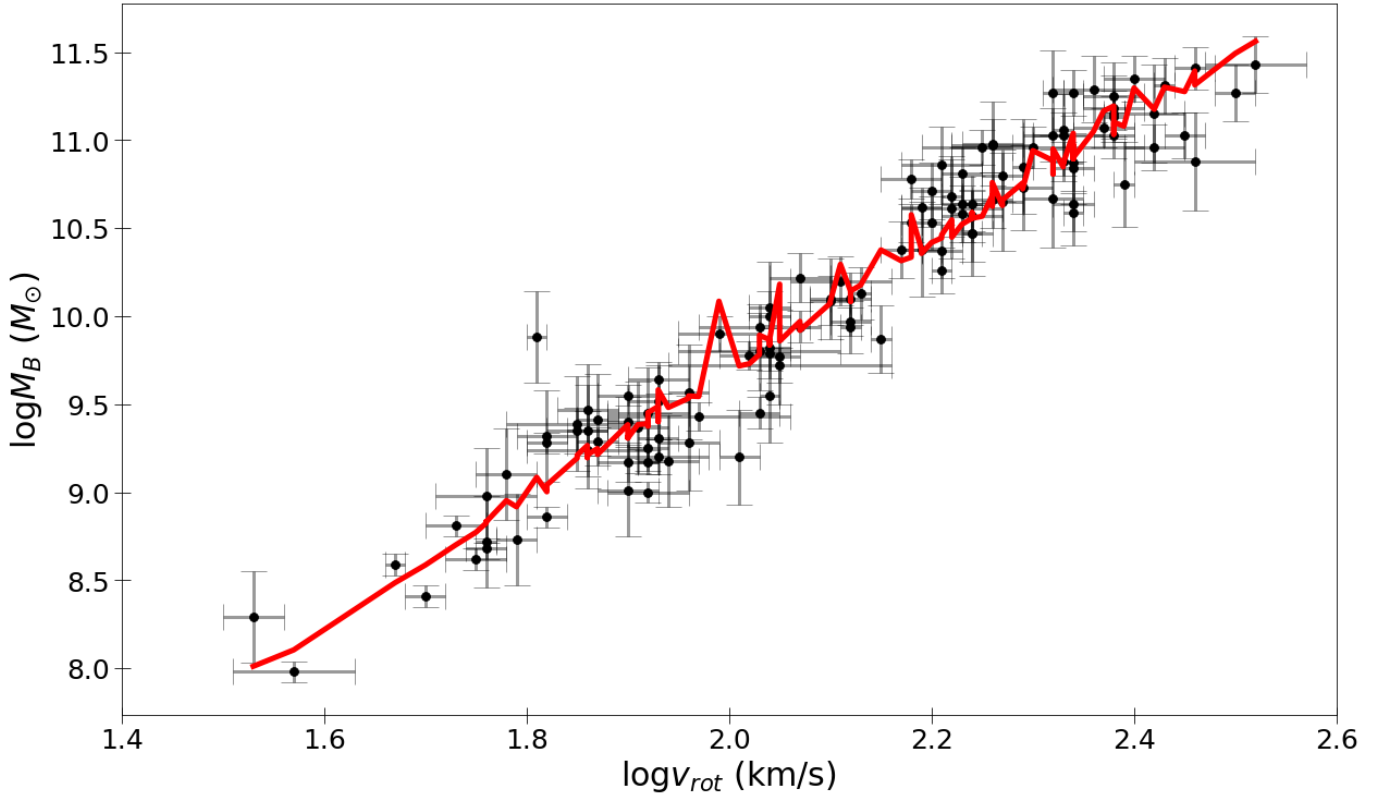


FIG. 2.— The best-fit line for the BTFR (using the fits in Fig. 1) along with the low-redshift data collated in A21. Note that the best-fit is also a function of distance which is not shown in this figure. However, the distance varies for each data point and that is why the curve shows some bumps and wiggles.

D (Mpc)	Slope	Intercept	$\ln \sigma_s$	χ^2/dof	p-value
< 9	3.38 ± 0.31	2.84 ± 0.58	$-1.50^{+0.21}_{-0.17}$	14.61/29	0.988
> 9	3.38 ± 0.17	3.05 ± 0.38	$-1.59^{+0.16}_{-0.13}$	43.71/83	1.000
< 17	3.47 ± 0.18	2.70 ± 0.35	$-1.48^{+0.16}_{-0.13}$	27.41/51	0.997
> 17	3.47 ± 0.21	2.86 ± 0.46	$-1.66^{+0.22}_{-0.15}$	31.67/61	0.999

TABLE 1

RESULTS FROM THE BEST-FIT BTFR PARAMETERS AFTER BIFURCATING THE SAMPLE AT 9 Mpc (FIRST TWO ROWS) AND 17 Mpc (LAST TWO ROWS) WITH THE INTRINSIC SCATTER AS A FREE PARAMETER. THE BEST-FIT PARAMETERS FOR BOTH THE SLOPE AND INTERCEPT ARE SEEN TO BE CONSISTENT BETWEEN BOTH THE SUBSAMPLES AT 1σ . THE χ^2/DOF FOR ALL FOUR SUBSAMPLES IS LESS THAN ONE AND p -VALUE IS ALSO CLOSE TO ONE, INDICATING THAT THERE IS NO STATISTICALLY SIGNIFICANT DIFFERENCES ACROSS THE SAMPLES.

find that the χ^2/dof is close to 1 and p -value is also > 0.1 for all the subsamples.

On splitting the dataset at 17 Mpc, we find that the p -value sample with $D > 17$ Mpc is close to one. However, the sample with $D < 17$ Mpc has a p -value of 0.04, equivalent to a 1.75σ discrepancy with respect to BTFR using the prescription in Cowan *et al.* (2011). It is likely that there are additional systematics in this data with $D < 17$ Mpc that have not been accounted for, which is a possible reason for the small p -value.

4. CONCLUSIONS

In a recent work, A21 used a dataset of 118 BTFR measurements at low redshifts ($z < 0.1$) to look for distance-dependent transitions in the parameters. They found a $3.7 - 4.5\sigma$ tension between the subsamples after splitting the data based on distance at 9 and 17 Mpc. This was ascertained based on the $\Delta\chi^2$ values of about 23.7 and 17, respectively. If this tension is interpreted as a change in the gravitational strength, it would imply a decrease in the effective Newton's constant of about 10%, which has the right sign and order of magnitude needed to resolve the Hubble tension conundrum in Cosmology.

In order to independently test this intriguing result, we did two analyses. We augmented the standard BTFR by adding a distance-dependent term in both the normalization and exponent (cf. Eq. 4). We fit the data in logarithmic space to this distance-dependent BTFR. The best-fit values for the distance-dependent terms in both slope and

D (Mpc)	Slope	Intercept	χ^2/dof	p-value
< 9	3.50 ± 0.19	2.61 ± 0.36	40.12/30	0.102
> 9	3.45 ± 0.13	2.88 ± 0.28	84.70/84	0.458
< 17	3.57 ± 0.10	2.51 ± 0.21	70.68/52	0.043
> 17	3.57 ± 0.15	2.64 ± 0.34	53.57/62	0.768

TABLE 2

RESULTS FROM THE BEST-FIT BTFR PARAMETERS AFTER BIFURCATING THE SAMPLE AT 9 MPC (FIRST TWO ROWS) AND 17 MPC KEEPING THE INTRINSIC SCATTER FIXED AT 0.077 SIMILAR TO A21.

intercept can be found in Fig. 1. The best-fit values for the distance-dependent slope (s) and intercept (b) are given by $s = -0.0078 \pm 0.0054$ and $b = 0.02 \pm 0.012$. Therefore, these parameters show only a mild variation with distance and are consistent with no variation within 2σ .

Finally, we bifurcated the dataset into two subsamples based on the distance at 9 and 17 Mpc, followed by analysis of the usual BTFR for these subsamples. The best-fit values are consistent across the subsamples. When we kept the intrinsic scatter as free parameter, the p -value of the fit is close to 1. When we used the same fixed value for the intrinsic scatter as A21, we the χ^2/dof for most of the subsamples is close to one. Only the subsample with $D < 17$ Mpc shows a marginal discrepancy with the BTFR with p -value equal to 0.043, corresponding to a 1.75σ discrepancy. However, this discrepancy is marginal and not large enough to claim a statistically significant tension between the two subsamples.

Therefore, we conclude that we cannot corroborate the results in A21 giving $> 3\sigma$ tension between the subsamples at the critical distances of 9 and 17 Mpc.

REFERENCES

- G. Alestas, I. Antoniou, and L. Perivolaropoulos, *Universe* **7**, 366 (2021), arXiv:2104.14481 [astro-ph.CO].
- R. B. Tully and J. R. Fisher, *A&A* **54**, 661 (1977).
- S. S. McGaugh, J. M. Schombert, G. D. Bothun, and W. J. G. de Blok, *ApJ* **533**, L99 (2000a), arXiv:astro-ph/0003001 [astro-ph].
- S. S. McGaugh, J. M. Schombert, G. D. Bothun, and W. J. G. de Blok, *ApJ* **533**, L99 (2000b), arXiv:astro-ph/0003001 [astro-ph].
- M. A. W. Verheijen, *ApJ* **563**, 694 (2001a), arXiv:astro-ph/0108225 [astro-ph].
- D. Zaritsky, H. Courtois, J.-C. Muñoz-Mateos, J. Sorce, S. Erroz-Ferrer, S. Comerón, D. A. Gadotti, A. Gil de Paz, J. L. Hinz, E. Laurikainen, T. Kim, J. Laine, K. Menéndez-Delmestre, T. Mizusawa, M. W. Regan, H. Salo, M. Seibert, K. Sheth, E. Athanassoula, A. Bosma, M. Cisternas, L. C. Ho, and B. Holwerda, *AJ* **147**, 134 (2014), arXiv:1402.6315 [astro-ph.GA].
- F. Lelli, S. S. McGaugh, and J. M. Schombert, *ApJ* **816**, L14 (2016), arXiv:1512.04543 [astro-ph.GA].
- B. Famaey and S. S. McGaugh, *Living Reviews in Relativity* **15**, 10 (2012), arXiv:1112.3960 [astro-ph.CO].
- S. S. McGaugh, F. Lelli, J. M. Schombert, P. Li, T. Visgaitis, K. S. Parker, and M. S. Pawlowski, *AJ* **162**, 202 (2021), arXiv:2109.03251 [astro-ph.GA].
- M. Aaronson, J. Huchra, and J. Mould, *ApJ* **229**, 1 (1979).
- F. Donato, G. Gentile, P. Salucci, C. Frigerio Martins, M. I. Wilkinson, G. Gilmore, E. K. Grebel, A. Koch, and R. Wyse, *MNRAS* **397**, 1169 (2009), arXiv:0904.4054 [astro-ph.CO].
- K. C. Freeman, *ApJ* **160**, 811 (1970).
- P. Salucci, *A&A Rev.* **27**, 2 (2019), arXiv:1811.08843 [astro-ph.GA].
- K. Gopika and S. Desai, *Physics of the Dark Universe* **30**, 100707 (2020), arXiv:2006.12320 [astro-ph.CO].
- K. Gopika and S. Desai, *Physics of the Dark Universe* **33**, 100874 (2021), arXiv:2106.07294 [astro-ph.CO].
- A. C. Mayer, A. F. Teklu, K. Dolag, and R.-S. Remus, arXiv e-prints, arXiv:2206.04333 (2022), arXiv:2206.04333 [astro-ph.CO].
- A. Paranjape and R. K. Sheth, *MNRAS* **507**, 632 (2021), arXiv:2102.13116 [astro-ph.GA].
- M. Kaplinghat and M. Turner, *ApJ* **569**, L19 (2002), arXiv:astro-ph/0107284 [astro-ph].
- S. McGaugh, *Galaxies* **2**, 601 (2014), arXiv:1412.3767 [astro-ph.GA].
- S. McGaugh, *Galaxies* **8**, 35 (2020), arXiv:2004.14402 [astro-ph.GA].
- S. Boran, S. Desai, E. O. Kahya, and R. P. Woodard, *Phys. Rev. D* **97**, 041501 (2018), arXiv:1710.06168 [astro-ph.HE].
- J. D. Bekenstein and E. Sagi, *Phys. Rev. D* **77**, 103512 (2008), arXiv:0802.1526 [astro-ph].
- C. Limbach, D. Psaltis, and F. Ozel, arXiv e-prints, arXiv:0809.2790 (2008), arXiv:0809.2790 [astro-ph].
- L. Portinari and J. Sommer-Larsen, *MNRAS* **375**, 913 (2007), arXiv:astro-ph/0606531 [astro-ph].
- H. Übler, N. M. Förster Schreiber, R. Genzel, E. Wisnioski, S. Wuyts, P. Lang, T. Naab, A. Burkert, P. G. van Dokkum, L. J. Tacconi, D. J. Wilman, M. Fossati, J. T. Mendel, A. Beifiori, S. Belli, R. Bender, G. B. Brammer, J. Chan, R. Davies, M. Fabricius, A. Galametz, D. Lutz, I. G. Momcheva, E. J. Nelson, R. P. Saglia, S. Seitz, and K. Takaki, *ApJ* **842**, 121 (2017), arXiv:1703.04321 [astro-ph.GA].
- M. Glowacki, E. Elson, and R. Davé, *MNRAS* **507**, 3267 (2021), arXiv:2011.08866 [astro-ph.GA].
- M. A. W. Verheijen, *ApJ* **563**, 694 (2001b), arXiv:astro-ph/0108225 [astro-ph].
- F. Walter, E. Brinks, W. J. G. de Blok, F. Bigiel, J. Kennicutt, Robert C., M. D. Thornley, and A. Leroy, *AJ* **136**, 2563 (2008), arXiv:0810.2125 [astro-ph].
- L. Verde, T. Treu, and A. G. Riess, *Nature Astronomy* **3**, 891 (2019), arXiv:1907.10625 [astro-ph.CO].
- E. Di Valentino, O. Mena, S. Pan, L. Visinelli, W. Yang, A. Melchiorri, D. F. Mota, A. G. Riess, and J. Silk, *Classical and Quantum Gravity* **38**, 153001 (2021), arXiv:2103.01183 [astro-ph.CO].
- S. Bethapudi and S. Desai, *European Physical Journal Plus* **132**, 78 (2017), arXiv:1701.01789 [astro-ph.CO].
- V. Marra and L. Perivolaropoulos, *Phys. Rev. D* **104**, L021303 (2021), arXiv:2102.06012 [astro-ph.CO].
- P. Zyla *et al.* (Particle Data Group), *PTEP* **2020**, 083C01 (2020).
- S. Bhagvati and S. Desai, *Classical and Quantum Gravity* **39**, 017001 (2022), arXiv:2108.05012 [gr-qc].
- S. Pradyumna, S. Gupta, S. Seeram, and S. Desai, *Physics of the Dark Universe* **31**, 100765 (2021), arXiv:2011.06421 [astro-ph.CO].
- D. Foreman-Mackey, D. W. Hogg, D. Lang, and J. Goodman, *PASP* **125**, 306 (2013), arXiv:1202.3665 [astro-ph.IM].
- A. Lewis, arXiv e-prints, arXiv:1910.13970 (2019), arXiv:1910.13970 [astro-ph.IM].
- S. Desai, *EPL (Europhysics Letters)* **115**, 20006 (2016), arXiv:1607.03845 [astro-ph.CO].
- G. Cowan, K. Cranmer, E. Gross, and O. Vitells, *European Physical Journal C* **71**, 1554 (2011), arXiv:1007.1727 [physics.data-an].

This paper was built using the Open Journal of Astrophysics L^AT_EX template. The OJA is a journal which provides fast and easy peer review for new papers in the `astro-ph` section of the arXiv, making the reviewing process simpler for authors and referees alike. Learn more at <http://astro.theoj.org>.